Dynamic Joint Simulation and Control of Hybrid Driven Three-degree-of-freedom Motor

Zheng Li[1], Lingqi Liu[1], Leiyong Wang[1]

[1]School of Electrical Engineering, Hebei University of Science and Technology, Shijiazhuang, China

Abstract

In order to solve the problem of complex motion coordination deviation and low flexibility of the existing drive unit in multi-rigid body coupling system, a new type of permanent magnet three-degree-of-freedom motor structure design is proposed, which is divided into inner deflection module and peripheral rotation modules. Their operating strategies can be divided into independent control and hybrid drive. By using the effect of strong magnetic and magnetic circuit shielding of Halbach array, the magnetic field characteristics of the motor's self-rotating permanent magnet are optimized and improved. Based on the construction of the joint simulation platform, the controlled object was derived by ADAMS software, and the control system was designed in MATLAB software. Aiming at the nonlinear and strongly coupled dynamic system, sliding mode control was selected as the dynamic control algorithm to study the trajectory tracking of the motor rotor shaft. By combining the dynamic model of the motor, the S function is written to complete the design of the controller. The simulation results show that the joint simulation interface and sliding mode control algorithm can well implement the trajectory tracking of hybrid drive motors.

Keywords: three-degree-of-freedom motor, Halbach array, virtual prototype; dynamic model, sliding mode control

Received: *19 February 2020*

To cite this article:
Zheng Li, Lingqi Liu, Leiyong Wang, "Electromagnetic Characteristics Analysis and Dynamics Co-simulation of Permanent Magnet Three-DOF Motor", in *Electrotehnica, Electronica, Automatica (E*EA), 2019, vol. 67, no. 3, pp. 13-21, ISSN 1582-5175. https://doi.org/10.46904/eea.20.68.3.1108002

1. Introduction

A complex and cumbersome multi-body mechanical system is often accompanied by a nonlinear, strongly coupled control method and multi-pattern, multi-degree-of-freedom motion conditions.

The transmission device composed of a plurality of conventional motors cooperates with each other, and the volumetric weight of the system is too large, and the mutual clearance of the plurality of bearings easily affects the rotation precision of the transmission [1]-[3].

Secondly, for the planning of complex multi-free movements, there will also be shortcomings such as slow response speed and poor transmission flexibility. To this end, domestic and foreign scholars have devoted themselves to the design and research of special motors with multiple rotational degrees of freedom in order to solve the above limitations. The multi-degree-of-freedom motor has many advantages such as compact size [4]-[7], compact structure, high material utilization rate and high mechanical integration, which greatly reduces the number of systems coupling mechanisms and further improves the accuracy of motor positioning motion [8]-[10].

In 1979, the American researcher K. Halbach was the first who proposed a new permanent magnet structure named Halbach array [9]. The magnetization direction was formed by a combination of radial and tangential directions and continuous change according to angle [10], which is usually considered in the manufacturing process. After the permanent magnets are divided into blocks [11]-[13], the angle between any adjacent magnets is kept the same, and the one-side effect of shielding on one side of the magnetic side is created, and a more sinusoidal air gap magnetic field and a smaller of torque fluctuations can be obtained [14]-[17].

At the same time, it can be seen from the references at home and abroad that the analysis and research of multi-degree-of-freedom motors mostly pay attention to the design of their body structure, but the motion control and trajectory planning of the three-degree-of-freedom of the motor are rarely involved [18]-[20].

When exploring the dynamic analysis of multi-degree-of-freedom motor, it mainly comes from the combination of mechanical design principle and classical theoretical mechanics [21].

However, due to the fast response motion characteristics of the motor during multi-degree-of-freedom motion, as well as bearing friction and external disturbance, the motor is caused. It is difficult to control

continuously, stably and accurately. Conventional PID control and torque control often fail to meet the requirements of trajectory tracking accuracy.

Therefore, based on the characteristics of strong coupling and nonlinearity of complex mechanical systems, a new intelligent control scheme suitable for multi-degree-of-freedom motors is proposed [22]. The parameters of the controlled object can be freely designed to reduce the sensitivity of the disturbance and make the control system more Good robustness.

2. Materials and Methods

2.1 Structural design and magnetic field distribution of a hybrid-driven motor

The proposed driving mechanism of the permanent magnet three-degree-of-freedom motor is hybrid drive type, including two types of electric modules, one is a rotation electric module, and the other is a deflection type electric module. The motor can independently complete the rotation and deflection operation according to the respective hinge constraints in the corresponding module, and complete the tilting operation and the rotating operation of the motor; it can start the rotation at the same time when the motor is deflected to a certain angle; it can also run to any Deflection at the same time, or in the cooperation of two different control strategies, realize three freedom of movement in the space.

Two fixed joints are fixed to the disc base by welding nails and bearing brackets, and two linkage joints are connected to the yoke of the deflection rotor by welding nails. The centre of the rotating stator yoke is provided with a circular hole for placing to cooperate with the rotation movement of the motor Rolling bearing, the cross connecting shaft is connected to the rotating rotor yoke in the axial direction, ends at the centre, and one end extends downward, embedded in the rolling bearing of the deflecting rotor yoke, fixed with the bearing inner ring, and can simultaneously carry radial And axial load; the other end extends upwards, as the external output shaft of the motor, which can maintain the linkage action on the output shaft during the overall model operation of the motor. The spherical bearing bracket is used to support the perforated shaft sleeve and the cross coupling, so that the deflection module is not limited to the deflection movement along the axis and can also realize multi-angle tilt operation. The overall model of the motor is shown in Figure 1.

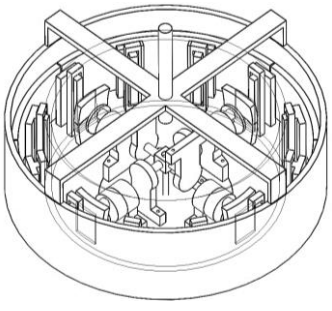

Figure 1. The overall model of the motor, the transmission, and the connecting shaft

In the structure that controls the motor's deflection movement, the inner rotor permanent magnets are set to 8 poles, 90 ° to each other, and a spherical patch is arranged up and down. The radial magnetization method in the spherical coordinate system is adopted. In the rotor yoke of the deflection module, the motor can be deflected after a certain time of the rotation operation.

One side of the deflection stator core is a drum type, which is suitable for four deflection permanent magnets.

The other side leads to three joints. The deflection stator coil is wound around the upper and lower joints of the stator core, opposite to the deflection stator core.

The inner side of the yoke is the deflection stator back yoke, which is fixedly connected to the deflection stator yoke by the intermediate joint of the deflection stator core.

One end of the stator bracket is connected to the deflection stator yoke, and the other end is connected to the disc base through the eight welding pins on the four sides. The base is fixed and plays the role of connecting the deflection stator.

In the structure that controls the rotation of the motor, the outer rotor permanent magnets are set to an 8-pole, ring-shaped columnar structure, arranged in the Halbach array in the vertical direction, and embedded in the outer rotor yoke, that is, the motor casing.

Each stage is divided into 3 pieces, and the magnetization direction of a single piece of permanent magnet in each stage changes sinusoidally along the circumferential direction. Together with the motor housing, it forms a rotation rotor, which can also achieve rotation when the motor is deflected to a certain angle.

The stator core of the rotation module of the drive motor is also distributed in a ring shape, and the rotation stator coil is wound around the salient pole portion of the stator core.

Maxwell's equations describing the relationship between magnetic field distribution and current are established by using the permanent magnet flux density B as the objective function under the solution domain.

$$\begin{cases} \nabla \cdot H(x,y,z) = J(x,y,z) \\ \nabla \cdot B(x,y,z) = 0 \end{cases} \tag{1}$$

The permanent magnet flux density is decomposed into three components in a Cartesian coordinate system, and multiplied by the unit vectors characterizing the three directions, and then added, the resulting vector form can be expressed as follows:

$$B(x,y,z) = B_x \cdot \vec{x} + B_y \cdot \vec{y} + B_z \cdot \vec{z} \tag{2}$$

The components of the air gap magnetic flux density in the motor rotation module and the deflection module are extracted, and after coordinate conversion, they are mapped to the cylindrical coordinate system and spherical coordinate system corresponding to the two types of drive modules, respectively,

And solved and calculated in the static magnetic field.

$$B_1 = \begin{pmatrix} B_{1r} \\ B_{1\varphi} \\ B_{1h} \end{pmatrix} = \begin{pmatrix} \cos\varphi & \sin\varphi & 0 \\ -\sin\varphi & \cos\varphi & 0 \\ 0 & 0 & 1 \end{pmatrix} \begin{pmatrix} B_{1x} \\ B_{1y} \\ B_{1z} \end{pmatrix} \quad (3)$$

$$B_2 = \begin{pmatrix} B_{2r} \\ B_{2\varphi} \\ B_{2\theta} \end{pmatrix} = \begin{pmatrix} \sin\theta\cos\varphi & \sin\theta\sin\varphi & \cos\theta \\ -\sin\theta & \cos\varphi & 0 \\ \cos\theta\cos\varphi & \cos\theta\sin\varphi & -\sin\theta \end{pmatrix} \begin{pmatrix} B_{2x} \\ B_{2y} \\ B_{2z} \end{pmatrix} \quad (4)$$

Among them, B_1 and B_2 are the air gap magnetic field density of the entire rotation module and the deflection module, B_{1r}, $B_{1\varphi}$, and B_{1h} are the three components of the rotation module in the cylindrical coordinate system, and B_{2r}, $B_{2\varphi}$, and $B_{2\theta}$ are the deflection modules in the spherical coordinate system of the three components. The magnetic field lines of the two types of permanent magnets of the motor are shown in Figure 2 and Figure 3.

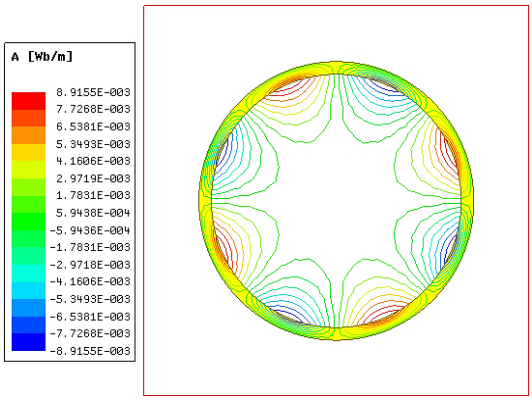

Figure 2. Magnetic field line distribution of a permanent magnet of a rotation module

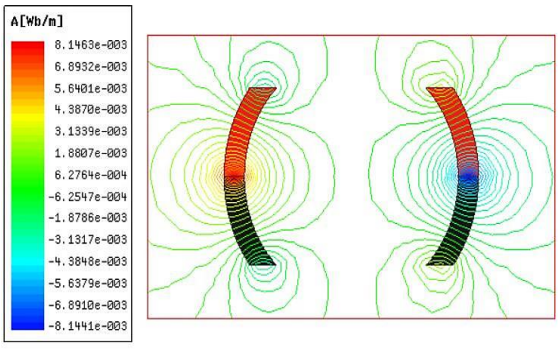

Figure 3. Magnetic field line distribution of a permanent magnet of a deflection module

2.2 Dynamic Model of hybrid drive motor

The default motor static axis coincides with the dynamic and static coordinate system at the static equilibrium position. The rotation sequence of 313 is used to move relative to the coordinate axis from O_{xyz} to x"y"z" respectively, which is regarded as the dynamic coordinate system O_{dpq}. The coordinate formulas for giving three rotations are as follows:

$$\begin{pmatrix} x \\ y' \\ z' \end{pmatrix} = \begin{pmatrix} 1 & 0 & 0 \\ 0 & \cos\alpha & \sin\alpha \\ 0 & -\sin\alpha & \cos\alpha \end{pmatrix} \begin{pmatrix} x \\ y \\ z \end{pmatrix} \quad (5)$$

$$\begin{pmatrix} x' \\ y' \\ z'' \end{pmatrix} = \begin{pmatrix} \cos\beta & 0 & -\sin\beta \\ 0 & 1 & 1 \\ \sin\beta & 0 & \cos\beta \end{pmatrix} \begin{pmatrix} x \\ y' \\ z' \end{pmatrix} \quad (6)$$

$$\begin{pmatrix} x'' \\ y'' \\ z'' \end{pmatrix} = \begin{pmatrix} \cos\gamma & \sin\delta & 0 \\ -\sin\gamma & \cos\delta & 0 \\ 0 & 0 & 1 \end{pmatrix} \begin{pmatrix} x' \\ y' \\ z'' \end{pmatrix} \quad (7)$$

In the rotating coordinate system, the angle between x" y" in the dynamic coordinate system and the N line vertically projected on the X0Y coordinate plane is α and β, and the angle between z " and the z axis is γ.

The coordinate formula of the three rotations in the above equations (5), (6), and (7) is combined, and the coordinate conversion formula and the transition matrix from the static coordinate system O_{xyz} to the dynamic coordinate system O_{dpq} are obtained. As shown in Figure (8) below.

$$\begin{pmatrix} x'' \\ y'' \\ z'' \end{pmatrix} = \begin{pmatrix} \cos\beta\cos\gamma & \sin\alpha\sin\beta\cos\gamma + \sin\gamma\cos\alpha & -\sin\beta\cos\alpha\cos\gamma + \sin\alpha\sin\gamma \\ -\cos\beta\sin\gamma & -\sin\alpha\sin\beta + \cos\alpha\cos\gamma & \sin\gamma\cos\alpha\cos\beta + \sin\alpha\cos\gamma \\ \sin\beta & -\sin\alpha\cos\beta & \cos\alpha\cos\beta \end{pmatrix} \begin{pmatrix} x \\ y \\ z \end{pmatrix} \quad (8)$$

In order to accurately characterize the relationship between the pose change of the rotor shaft of the motor and the externally applied three-direction torque, all the rotor parts are regarded as the same linked rigid body, and are derived according to the second type equation of Lagrangian mechanics as follows:

$$\frac{d}{d_t}\left(\frac{\partial E}{\partial \dot{q}_j}\right) - \frac{\partial E}{\partial \dot{q}_j} = Q_j, (j = 1,2,3.....,n) \quad (9)$$

where

E is the kinetic energy of the local dynamic coordinate system;

q_j is the jth action point in the dynamic coordinate system;

Q_j is the rotational moment applied under the action point q_j.

When the motor moves to any posture under the action of three driving torques, there is a rotation coordinate $(\alpha,\beta,\gamma)^T$ corresponding to the Euler parameter. The angular velocity of rotation of the rotor shaft of the motor along the axis is represented by a vector form of $w=(w_x,w_y,w_z)T$. According to the conversion relationship of the dynamic coordinate system to the static coordinate system, set $(\dot{\alpha},\dot{\beta},\dot{\gamma})T$ as the angular velocity under the rotation coordinate $(\alpha,\beta,\gamma)^T$. The angular velocity of rotation in the kinetic calculation can be represented by a transition matrix in rotational coordinates:

$$\begin{pmatrix} w_1 \\ w_2 \\ w_3 \end{pmatrix} = \begin{pmatrix} \cos\beta\cos\gamma & \sin\gamma & 0 \\ -\cos\beta\sin\gamma & \cos\gamma & 0 \\ \sin\beta & 0 & 1 \end{pmatrix} \begin{pmatrix} \dot{\alpha} \\ \dot{\beta} \\ \dot{\gamma} \end{pmatrix} \quad (10)$$

In the case of the three-degree-of-freedom movement of the motor, the condition that the degree of freedom of the mechanical system is greater than the value of the constrained drive is required, and there are three unconstrained degrees of freedom, that is, n=3.

The generalized local coordinate points are $q_1=a$, $q_2=\beta$, $q_3=\gamma$, and the generalized driving torque is $Q_1=\tau_a-\tau_{fa}$, $Q_2=\tau_\beta-\tau_{f\beta}$, and $Q_3=\tau_\delta-\tau_{f\delta}$. In the formula, τ_a, τ_β, and τ_δ represent that the rotor shaft of the motor is affected by the internal load, and the driving torque in the deceleration braking period is the magnitude of three axis components.

Taking the Cartesian global coordinate system as the stationary coordinate system, the kinetic energy of the rotation and deflection parts of the hybrid drive motor when they are synchronized is:

$$E = \frac{1}{2}J_d w_1^2 + \frac{1}{2}J_q w_2^2 + \frac{1}{2}J_p w_3^2 \quad (11)$$

Let $J = \begin{pmatrix} J_d & J_{xy} & J_{xz} \\ J_{yx} & J_p & J_{yz} \\ J_{zx} & J_{zy} & J_q \end{pmatrix}$ be the inertia tensor matrix of the rotor part of the motor to reflect the inertia of the inner and outer rotors in the rigid body system. When the motor moves freely, the rotation along different axes in the relative static coordinate system is the difference is that it is necessary to determine the axis that describes its relative motion. J_d, J_p and J_q are the permanent magnet three-degree-of-freedom motor in the local motion coordinate system *dpq*, respectively, for the X-axis, Y-axis, Z-axis spindle moment of inertia, the remaining inertia products are 0.

And since the overall model of the motor is symmetric about the two coordinate planes of X0Z and YOZ, then $J_d=J_p\neq J_q$. Here is the order $J_d=J_p=J_{dp}$. Combine the above kinetic energy expressions as follows:

$$E = \frac{1}{2}J_{dq}(w_1^2 + w_2^2) + \frac{1}{2}J_q w_3^2 \quad (12)$$

Combine the above formula (12) and substitute it to:

$$\begin{aligned} &(J_{dq}\cos^2\beta + J_q\sin^2\beta) + J_q\ddot{\gamma}\sin\beta \\ &+ 2(J_q - J_{dq})\dot{\alpha}\dot{\beta}\cos\beta\sin\beta + J_q\dot{\beta}\dot{\gamma}\cos\beta = \tau_{\beta-\tau_{f\beta}} \end{aligned} \quad (13)$$

$$J_q\ddot{\gamma}\sin\beta + J_q\ddot{\gamma} + J_q\dot{\alpha}\dot{\beta}\cos\beta = \tau_r - \tau_{fr}$$

The dynamic mathematical model of the multi-degree-of-freedom motor is mainly used to better describe the driving torque applied in the three directions of the motor and the pose change of the components in the rotation and deflection modules.

Establish a mathematical model of the three-degree-of-freedom dynamics of a hybrid-driven motor in space.

$$H(q)\ddot{q} + C(q,\dot{q})\dot{q} = \tau \quad (14)$$

Among them,

$$H(q) = \begin{pmatrix} H_{11} & H_{12} & H_{13} \\ H_{21} & H_{22} & H_{23} \\ H_{31} & H_{32} & H_{33} \end{pmatrix}$$

is the inertia matrix of the rotor output shaft, τ is the matrix of the combined component torque, $q=(a,\beta,\gamma)^T$ is the column vector of the Euler rotation angle, and

$$C(q,\dot{q}) = \begin{pmatrix} C_{11} & C_{12} & C_{13} \\ C_{21} & C_{22} & C_{23} \\ C_{31} & C_{32} & C_{33} \end{pmatrix}$$

is the Coriolis centrifugal force matrix.

$$\begin{cases} H_{11} = J_{dq}\cos^2\beta + J_p\sin^2\beta \\ H_{12} = 0 \\ H_{13} = J_q\sin\beta \\ H_{21} = 0 \\ H_{22} = J_{dq} \\ H_{23} = 0 \\ H_{31} = J_q\sin\beta \\ H_{32} = 0 \\ H_{33} = J_q \end{cases} \quad (15)$$

After solving the established dynamic equation, the coefficients of the inertia matrix and the Coriolis centrifugal force matrix are as follows. The components of the inertia matrix are shown in equation (15), and the parameters of the Coriolis centrifugal force matrix are shown in equation (16).

From the equations, the effects of cross coupling can be clearly shown, which is just similar with the characteristics of robotics and spatial motion mechanisms and the simulation and control can be referred from them.

$$\begin{cases} C_{11} = (J_q - J_{dq})\dot{\beta}\sin\beta\cos\beta \\ C_{12} = (J_q - J_{dq})\dot{\alpha}\sin\beta\cos\beta + \frac{1}{2}J_p\dot{\gamma}\cos\beta \\ C_{13} = \frac{1}{2}J_p\dot{\beta}\cos\beta \\ C_{21} = (J_{dp} - J_q)\dot{\alpha}\sin\beta\cos\beta - \frac{1}{2}J_p\dot{\gamma}\cos\beta \\ C_{22} = 0 \\ C_{23} = -\frac{1}{2}J_p\dot{\alpha}\cos\beta \\ C_{31} = \frac{1}{2}J_p\dot{\beta}\cos\beta \\ C_{32} = \frac{1}{2}J_p\dot{\alpha}\cos\beta \\ C_{33} = 0 \end{cases} \quad (16)$$

2.3 Dynamic Co-simulation Based on Cooperative Control of Hybrid Driven Motors

A ball hinge is added at the boundary between the spherical inner bearing and the perforated bushing of the motor, and three directions of rotational torque are applied as the torque for driving the motor three free movements. The remaining inner and outer rotors are connected by a fixed pair and are regarded as a linkage, which moves as the output shaft moves. By giving different forms of drive torque, the hybrid drive motor can be moved in a variety of three degrees of freedom around its static equilibrium point. Based on the three-degree-of-freedom motion of the ball hinge, the three slip degrees of freedom are constrained, and the axial torque of the three vertical coordinate planes is applied, and then the three-degree-of-freedom dynamics simulation of the motor is realized.

In order to reflect the linkage control of the motor in cooperation with the rotation module and the deflection module, a typical three-degree-of-freedom motion condition trajectory under dynamics is planned. At the same time, the rocking motion around the left and right sides of the z-axis and the tilting motion deviating from the z-axis are realized, which are synthesized into a lightning-type motion that reciprocates three times. Drive torque as shown in Figure 4 below.

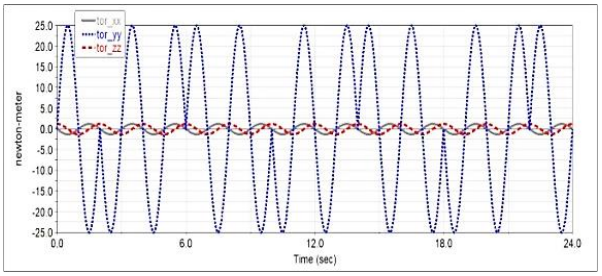

Figure 4. "Helical" motion trajectory and axial angle monitoring of the motor

The simulation time is set to 24 seconds, the number of simulation steps is 1500, three axial torques are given by the nested IF function, and the driving torque around the x-axis and the z-axis is controlled to be a sine and cosine variation of the equal amplitude, phase The difference is 90 °, and then the motor is driven to complete the arc offset of each reciprocating motion; the torque around the y-axis is controlled to be a periodic sinusoidal change, wherein each 8 s is a period, and the interval is divided by 2 s in each period. The torque direction is cycled three times in the order of "+--+", and the lightning-type trajectory of the motor reciprocating three times around the y-axis is completed.

As shown in Figure 5 below, under the combined action of the above three axial driving torques, the lightning-type motion trajectory of the motor can be realized.

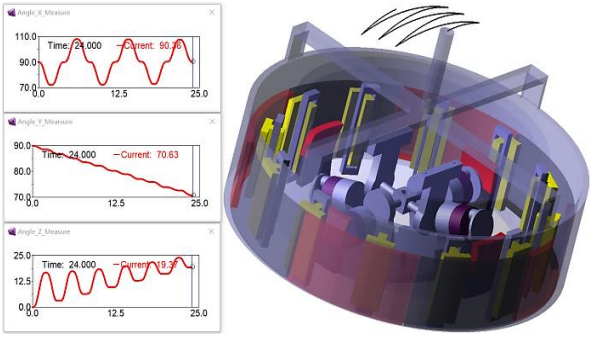

Figure 5. Lightning motion trajectory and axial angle monitoring of the motor

It can be used for the processing of heterogeneous complex mechanical parts, and the complicated path that cannot be realized by single-degree-of-freedom motor and has special requirements. For example, when the glass wire of the shaped glass member is wound, the obstacle can be effectively avoided.

At the same time, the three axial angles are measured in real time. By adjusting the motor moment of inertia, the driving torque and the position of the centroid point, the angle between the x and y axes of the motor is limited to 20° when the motor is engaged in lightning motion. The z axial angle is limited to 25 °.

Based on the virtual prototype technology and the control system process for collaborative control, an interface module for dynamic joint simulation is established, 6 state variables are created, 3 axial drive torques are set as input variables, 3 axial angular speeds are output variables, and The external load corresponding to the motor model is electrically related. Set the corresponding control parameters and generate the corresponding joint simulation file after export.

First, three axial torques are applied to the hybrid drive motor, and the three axial angular velocities obtained after open-loop control are used as inputs. At the same time, the axial angle and axial angular acceleration of the motor are obtained through the integral and differential links. It is used to cooperate with the design of subsequent controllers; secondly, the dynamic control algorithm is written by the S function to obtain the dynamic control law, so as to output the axial torque. At the same time, the three axial torques are also used as the input of the joint simulation. After the joint simulation interface is output, the axial angular velocity is fedback and the input axial angle is fed back to achieve closed-loop control of trajectory tracking of the hybrid drive motor.

Take the lightning trajectory of the motor as an example. Based on the virtual prototyping technology and the control system flow, the interface module of the dynamic co-simulation is established, six state variables are created, three axial driving torques are set as input variables, and three axial angular velocities are output variables. The external load corresponding to the motor model produces an electrical correlation. Three input/output interfaces are determined and exported in the form of mechanical system sub-modules to generate a virtual prototype model, adams_sub, of the hybrid

drive motor. The virtual prototype model of a hybrid-driven three-degree-of-freedom motor is shown in Figure 6.

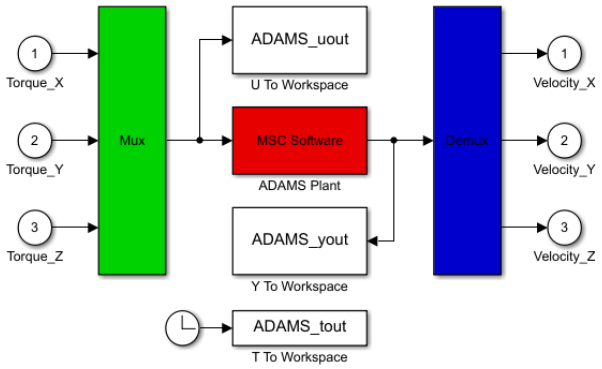

Figure 6. Virtual prototype model of hybrid drive motor

Set to discrete, interactive operation mode, the three axial drive torques of the motor are taken as input functions, and the three axial angular velocities of the motor are obtained through the virtual prototype model adams_sub as the controlled object and complete the following dynamic open loop control simulation.

At the same time, the three axial angular velocities of the motor are stored as synchronous simulation data to three specific working spaces, which facilitates the subsequent trajectory tracking control of the motor.

The mathematical model of the dynamics of a hybrid drive motor is:

$$M(W)\dot{W}+C(W,\dot{W})W=\tau \tag{17}$$

Let $H(W,\dot{W})=C(W,\dot{W})W$, it can be expressed as follows:

In the above formula, $w=[w_1,w_2,w_3]^T$ is the angle value of the feedback, and $w^d=\left[w_1^d,w_2^d,w_3^d\right]^T$ is the given angle value; $\dot{w}=[\dot{w}_1,\dot{w}_2,\dot{w}_3]^T$ is the angular velocity value of the feedback, and $\dot{w}=\left[\dot{w}_1^d,\dot{w}_2^d,\dot{w}_3^d\right]^T$ is the given angular velocity value.

Set the trajectory tracking error function to be: $s=Ke+\dot{e}$.

Here, $K=\begin{bmatrix}K_1 & & \\ & K_2 & \\ & & K_3\end{bmatrix}$, and after the error function is derived, you can get:

$$\dot{s}=\begin{bmatrix}k_1\dot{e}_1+\ddot{e}_1\\ k_2\dot{e}_2+\ddot{e}_2\\ k_3\dot{e}_3+\ddot{e}_3\end{bmatrix}=\begin{bmatrix}k_1\dot{e}_1\\ k_2\dot{e}_2\\ k_3\dot{e}_3\end{bmatrix}+\begin{bmatrix}\ddot{w}_1^d\\ \ddot{w}_2^d\\ \ddot{w}_3^d\end{bmatrix}-\begin{bmatrix}\ddot{w}_1\\ \ddot{w}_2\\ \ddot{w}_3\end{bmatrix}$$

$$=\begin{bmatrix}k_1\dot{e}_1\\ k_2\dot{e}_2\\ k_3\dot{e}_3\end{bmatrix}+\begin{bmatrix}\ddot{w}_1^d\\ \ddot{w}_2^d\\ \ddot{w}_3^d\end{bmatrix}-M^{-1}(\tau-H) \tag{18}$$

Select to approach the sliding surface at an equal rate:

$$\dot{s}=-\varepsilon sgn(s)=\begin{bmatrix}-\varepsilon_1 sgn(s_1)\\ -\varepsilon_2 sgn(s_2)\\ -\varepsilon_3 sgn(s_3)\end{bmatrix} \tag{19}$$

In the above formula, ε is the degree of speed of the multi-degree-of-freedom motion of the virtual prototype model to approximate the slip surface s=0. The value of ε directly affects the rate at which any point in the motor's motion trajectory reaches the sliding surface. If the value of ε is too large, the corresponding "chattering" will be larger.

After the above finishing, the control law of joint simulation can be obtained as follows:

$$\tau=M\left(\begin{bmatrix}k_1\dot{e}_1\\ k_2\dot{e}_2\\ k_3\dot{e}_3\end{bmatrix}+\begin{bmatrix}\ddot{w}_1^d\\ \ddot{w}_2^d\\ \ddot{w}_3^d\end{bmatrix}+-\varepsilon sgn(s)\right)+H \tag{20}$$

When the virtual prototype based on hybrid drive motor realizes the cooperative control of the rotation motion and the yaw motion, it is likely that large eccentric displacement and bearing friction and other uncertain factors will occur, which will further weaken the damage of the chatter control system stability.

The saturation function *sat*(*s*) is used to replace the symbol function *sgn*(*s*) in the controller, and linear feedback is used inside the boundary layer to form a smooth approaching effect near the switching surface. As follows:

$$sat(s)=\begin{cases}1 & s>\Delta\\ ks & |s|\le\Delta \quad k=1/\Delta\\ -1 & s<-\Delta\end{cases} \tag{21}$$

In the above formula (24), Δ is a boundary layer of the sliding surface.

After the substitution of equation (22), the final control law of the co-simulation system is:

$$\tau=M\left(\begin{bmatrix}k_1\dot{e}_1\\ k_2\dot{e}_2\\ k_3\dot{e}_3\end{bmatrix}+\begin{bmatrix}\ddot{w}_1^d\\ \ddot{w}_2^d\\ \ddot{w}_3^d\end{bmatrix}+-\varepsilon sat(s)\right)+H \tag{22}$$

Set the dynamics system stability function to:

$$V=\frac{1}{2}ss^T \tag{23}$$

After the formula (24) is derived, it is:

$$\dot{V}=ss=s\left(\begin{bmatrix}k_1\dot{e}_1\\ k_2\dot{e}_2\\ k_3\dot{e}_3\end{bmatrix}+\begin{bmatrix}\ddot{w}_1^d\\ \ddot{w}_2^d\\ \ddot{w}_3^d\end{bmatrix}-M^{-1}(\tau-H)\right) \tag{24}$$

Substituting equation (25) is:

$$\dot{V} = -\varepsilon sat(s)s \tag{25}$$

when $\varepsilon > 0$, $\dot{v} \le 0$, the co-simulation control system tends to be stable.

3. Results

Faced with uncertainties such as input disturbance, bearing friction, and parameter perturbation, the sliding mode variable structure control algorithm with invariance, high reliability and good robustness was selected. Combined with the dynamic mathematical model of the hybrid drive motor, based on the real-time data exchange between the virtual prototype and the control system under collaborative control, a machine-control integrated control simulation platform is established. The controller algorithm design of the motor is completed by writing S-Function.

The virtual prototype model of the hybrid drive motor was used as the controlled object. The three axial angular velocities, three axial angles, and three axial angular accelerations obtained before the open-loop control were used as the given nine input quantities. The three axial angular velocities and three axial angular outputs output by the virtual prototype model are used as the six input quantities for feedback.

It can be seen that the change trend of the error is roughly equivalent to the change trend of the angular velocity. The tracking error range of the dynamic trajectory tracking of the motor x and z axis angular velocity is -0.0012-0.0012 rad/s, and the tracking error range of the y axis angular velocity is -0.015-0.015. Around rad/s, the error between the output response and the input signal is about 2.5 %, which proves that the sliding mode control is good, and the design of the controller can effectively track the trajectory of the output shaft.

When running the simulation, set the simulation time to 24 s and the communication time to 0.05 s. With the constant change of the control parameters, the sliding mode surface finally converges to 0.

As shown in Figure 7, the angular velocity curves correspond to the y-axis of the "folded-line" motion trajectory of the hybrid drive motor under joint simulation.

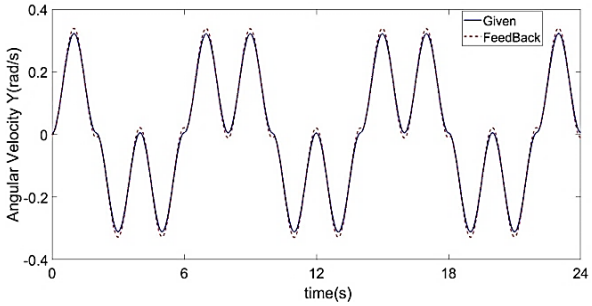

Figure 7. Axial angular velocity tracking under sliding mode control

It can be seen that the feedback signal of the three axial angular velocities at the beginning of the movement can track the input signal with almost no delay time, except that the change trend of the output response has a certain trend at the inflection point. In addition to jitter, the tracking effect can be achieved during the entire dynamic control period.

4. Discussion

As shown in Figure 8, the experimental platform for the multi-degree-of-freedom motor is built.

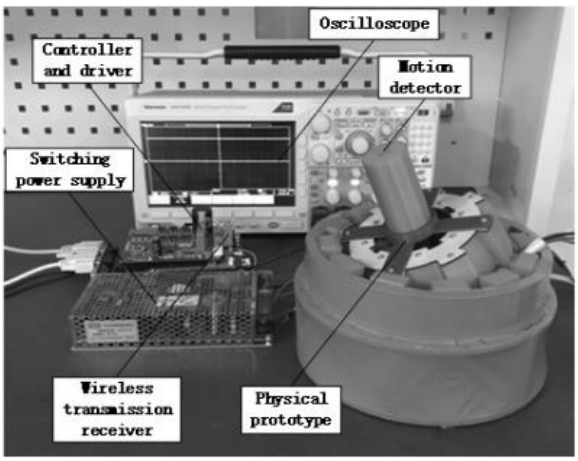

Figure 8. Experimental test of the motor

The control algorithm is downloaded to the controller, and the external rotation module is connected to the three-phase power frequency alternating current to realize the rotation operation of the motor. The switching power supply is connected to the deflection module, and the direct current of 5A is input. Under the synergy of the two types of drive modules, the motor is controlled by the modulation of the controller and the drive to realize a three-degree-of-freedom "lightning type" obstacle avoidance movement. The end of the motor output shaft is equipped with a displacement sensor.

The collected data is input to the controller through the wireless transmission module, and the controller data is exported to the MATLAB to draw the motion track and compared with the previous simulation results.

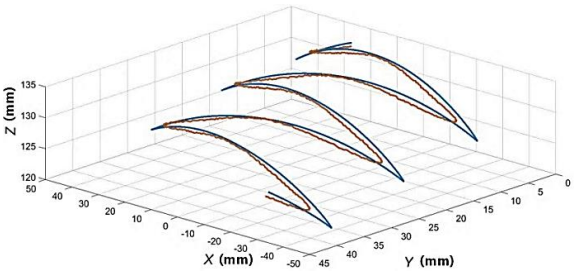

Figure 9. Comparison of experimental test and simulation

As shown in Figure 9, Figure a and b show the three-dimensional curve of the end point of the motor output shaft and the two-dimensional trajectory projected on the XOY coordinate plane. The red curve is the displacement change of the experimental test. The blue curve is the displacement change of the dynamic

simulation. It can be seen that the displacement of the dynamic simulation trajectory is a three-time shift starting at the static equilibrium position, and the displacement of the tracking trajectory has basically no change in the tilting movement away from the z-axis.

There are fluctuations in the rocking motion around the z-axis left and right sides. Compared with the dynamic simulation planning trajectory offset to the point position, it is smoother and has a certain deviation, but the overall trend and the dynamic simulation trajectory trend is consistent.

5. Conclusions

This paper proposes a new hybrid drive type three-degree-of-freedom motor. Taking the 12/8 pole fixed rotor of the external rotation module and the 8/4 pole fixed rotor of the internal deflection module as examples, the Halbach array magnetization method in the cylindrical coordinate system is used for the rotation permanent magnet of the motor. The three-degree-of-freedom motion of the space is planned under the constraint of the ball hinge, and the variation range of the angle value with the three axes and the trend of the displacement change are detected, which proves the rationality and practicability of the motor to realize the three-degree-of-freedom motion. It provides more theoretical basis for the subsequent manufacture and testing of physical prototypes and maximizes cost savings. By combining the dynamic mathematical model of the three-degree-of-freedom motor, a joint simulation platform based on the sliding mode control system is built to realize the trajectory tracking of the three axial angular velocities of the motor.

Finally, a hybrid-driven multi-freedom motor control platform was built. Aiming at the problem of tracking the rotor shaft displacement, the comparison between physical tests and simulations verified the correctness of the control algorithm and the prototype.

6. Bibliographic References

[1] ZE ZHOU, Y., JIAN JUN, S., YI T., et al. "An Integrated Dual Voltage Loop Control for Capacitance Reduction in CHB-Based Regenerative Motor Drive Systems", in IEEE Transactions on Industrial Electronics, 2019, vol. 66, no. 5, pp. 3369-3379. ISSN: 0278-0046.

[2] BIN, L., JING, Z., XIANG DONG, L., et al. "Detent Force Reduction of an Arc-Linear Permanent-Magnet Synchronous Motor by Using Compensation Windings", in IEEE Transactions on Industrial Electronics, 2017, vol. 64, no. 4, pp. 3001-3011, ISSN 0278-0046.

[3] HAN, D., MORRIS, C.T., Sarlioglu, B. "Common-Mode Voltage Cancellation in PWM Motor Drives With Balanced Inverter Topology", in IEEE Transactions on Industrial Electronics, 2017, vol. 64, no. 1, pp. 2683-2688, ISSN 0278-0046.

[4] HUAWEI, Z., WENXIANG, Z., GUOHAI, L., et al. "Remedial Field-Oriented Control of Five-Phase Fault-Tolerant Permanent-Magnet Motor by Using Reduced-Order Transformation Matrices", IEEE Transactions on Industrial Electronics, 2017, vol. 64, no. 1, pp. 169-178, ISSN 0278-0046.

[5] GMYREK, Z., LEFIK, M. "Influence of Geometry and Assembly Processes on the Building Factor of the Stator Core of the Synchronous Reluctance Motor", in IEEE Transactions on Industrial Electronics, 2017, vol. 64, no. 4, pp. 2443-2450, ISSN 0278-0046.

[6] MARTIN, S.C., WHITCOMB, L.L. "Nonlinear Model-Based Tracking Control of Underwater Vehicles With Three Degree-of-Freedom Fully Coupled Dynamical Plant Models: Theory and Experimental Evaluation", in IEEE Transactions on Control Systems Technology, 2018, vol. 26, no. 2, pp. 404-414, ISSN 1063-6536.

[7] TING NA, S., XIN, X., CHANG LIANG, X. "Improved Deviation Coupling Multi-motor Synchronous Control Using Virtual Motor", in Proceedings of the CSEE, 2017, vol. 37, no. 23, pp. 7004-7013.

[8] NING, L., CHANG LIANG, X., ZHANQING, Z., et al. "Speed Smoothing Control of Permanent Magnet Synchronous Motor Based on Proportional Gain Compensation", in Transactions of China Electrotechnical Society, 2018, vol. 37, no. 17, pp. 4007-4015.

[9] Fischer N, Johnson B K, Miles A G, et al. "Induction Motor Modeling for Development of a Secure In-Phase Motor Bus Transfer Scheme", in IEEE Transactions on Industry Applications, 2018, vol. 55, no. 1, pp. 203-212. ISSN: 0093-9994

[10] DEV, C.M., FIRDADUSA, A., GAURAV, K., et al. "Design methodology for a special single winding based bearingless switched reluctance motor", in The Journal of Engineering, 2017, no. 23, pp. 274-284, ISSN: 2051-3305.

[11] CHINELLO, F., PACCHIEROTTI, C., MALVEZZI, M., et al. "A Three Revolute-Revolute-Spherical wearable fingertip cutaneous device for stiffness rendering", in IEEE Transactions on Haptics, 2018, vol. 11, no. 1, pp. 39-50, ISSN 1939-1412.

[12] ZHENG, L., QING QING, L., ZENG TAO, X., et al. "Calculation and Analysis of Magnetic Field and Torque Characteristics of Three-DOF Motor with Permanent Magnet Rotor Deflection", in Transactions of Electrical Engineering, 2017, vol. 32, no. 23, pp. 81-90.

[13] YUE FEI, Z., JIE, Z., WEI L., et al. "Improved Active Disturbance Rejection Controller for Permanent Magnet Synchronous Motors with Time-varying Input", in Transactions of Electrical Engineering, 2017, vol. 32, no. 2, pp. 161-170.

[14] BO, Y., SHOU TONG, T., LING, H., et al. "Joint simulation of myoelectric artificial hand based on MATLAB and ADAMS", in Journal of System Simulation, 2017, vol. 29, no. 5, pp. 958-964.

[15] HONG FENG, L., TING MENG, L. "End-Effect Magnetic Field Analysis of the Halbach Array Permanent Magnet Spherical Motor", in IEEE Transactions on Magnetics, 2018, vol. 54, no. 4, pp. 1-9.

[16] JIAN NING, D., YUN KAI, H., LONG, J., et al. "Thermal Optimization of a High-Speed Permanent Magnet Motor" in IEEE Transactions on Magnetics, 2014, vol. 50, no. 2, pp. 749-752.

[17] DAS P K., BEHERA H S., PANIGRAHI B K. "A hybridization of an improved particle swarm optimization and gravitational search algorithm for multi-robot path planning [J]", Swarm and Evolutionary Computation, 2016, vol. 28, no. 4, pp. 14-28.

[18] HONG FENG, L., YAN BO, S. "Thermal Analysis of the Permanent-Magnet Spherical Motor", in IEEE Transactions on Energy Conversion, 2015, vol. 30, no. 3, pp. 1-8.

[19] QUN JING, W., ZHENG, L., WEI, X., et al. "Calculation and Analysis of Structural Parameters and Torque Characteristics of a Novel Permanent Magnet Spherical Stepper Motor", in Proceedings of the CSEE, 2006, vol. 26, no. 10, pp. 158-165.

[20] GUO, X., QUN JING, W., ZHENG, L., et al. "Adaptive Fuzzy Control of Permanent Magnet Spherical Motor Based on Friction Compensation", in Proceedings of the CSEE, 2011, vol. 31, no. 15, pp. 75-81.

[21] FERNANDES, J.F.P., VIEIRA S.M., BRANCO P.J. "Multi-Objective Optimization of a Shell-like Induction Spherical Motor for Power-Assisted Wheelchair", in IEEE Transactions on Energy Conversion, 2017, vol. 33, no. 2, pp. 660-669, ISSN: 0885-8969.

[22] BAI, K., XU, R., LEE, K M., et al. "Design and Development of a Spherical Motor for Conformal Printing of Curved Electronics [J]", in IEEE Transactions on Industrial Electronics, 2018, 65(11):9190-9200.

[23] DUQUE, J., GREENHOUSE, I., LABRUNA L., et al. "Physiological Markers of Motor Inhibition during Human Behaviour", in Trends in Neurosciences, 2017, vol. 40, no. 4, pp. 219-236.
[24] EMBORG M.E., MA S.Y., MUFSON E.J., et al. "Age-related declines in nigral neuronal function correlate with motor impairments in rhesus monkeys", in Journal of Comparative Neurology, 2015, vol. 401, no. 2, pp. 253-265.
[25] XIWEN, G., SHEN, L., QUNJING, W., et al. "continuous trajectory planning of permanent magnet spherical motor by cubic spline interpolation", in *Electrotehnica, Electronica, Automatica (EEA)*, 2017, vol. 65, no. 3, pp. 70-75.

Funding Sources

This work was financially supported by the National Natural Science Foundation of China (51877070, 51577048); Hebei Provincial Natural Science Foundation Project (E2018208155); the Talent Engineering Training Support Project of Hebei Province (A201905008); Hebei Province Higher Education Science and Technology Research Key Project (ZD2018228); High-energy-saving Motor and Control Technology National and Local Joint Engineering Laboratory Open Project (KFKT201901), Hebei Province Graduate Innovation Funding Project (CXZZSS2018085, CXZZSS2019084).

Authors' Biographies

Zheng Li was born in Shijiazhuang (China), on January3, 1980.
He received the PhD. degree in power electronics and electrical drive from Hefei University of Technology (China), in 2007.
Currently, he is a Professor at Hebei University of Science and Technology, in Shijiazhuang (China).
His major research interests concern: design, analysis, and control of novel motors and actuators, intelligent control, and power electronics.
e-mail address: Lizheng@hebust.edu.cn; Lzhfgd@163.com

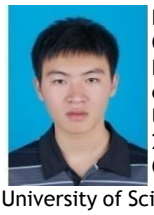

Lingqi Liu was born in Shijiazhuang (China), on October 14, 1993.
He received the B.Sc. degree in electrical engineering and automation from Hebei University of Science and Technology (China), in 2017.
Currently, He is a graduate student at Hebei University of Science and Technology, in Shijiazhuang (China).
His major research interests concern: Design and control technology of multi-degree-of-freedom motor
e-mail address: liulingqi@stu.hebust.edu.cn

Leiyong Wang was born in Changzhou (China), on April 21, 1984.
He received the B.Sc. degree in electrical engineering and automation from Hebei University of Science and Technology (China), in 2017.
Currently, he is a graduate student at Hebei University of Science and Technology, in Shijiazhuang (China).
He major research interests concern: special motor control and linear motor drive.
e-mail address: wangleiyong@stu.hebust.edu.cn

ELECTROTEHNICĂ, ELECTRONICĂ, AUTOMATICĂ (EEA), 68 (2020), nr. 3, pp. 22-31
https://doi.org/10.46904/eea.20.68.3.1108003

Modelling and Simulation of a Brushless Motor DC for Electric Power Steering Assistance

Daniela CIOBOATĂ[1], Mihăiță Gabriel NEACȘU[2], Dănuț STANCIU[1], Silviu Ștefan MATEI[2], Irina NEACȘU[2]

[1]**Institutul Național de Cercetare-Dezvoltare pentru Mecatronică și Tehnica Măsurării (INCDMTM)**, Șos. Pantelimon, nr. 6-8, 021631 București, Romania
[2]Icpe, Splaiul Unirii, nr. 313, 030138, București, Romania

Abstract

This paper presents an approach to develop a brushless DC motor to assist an electric power steering. Optimal design for electric power steering system implies the adequate selection of topology, technology, sizes and control algorithm. This paper briefly describes the electric power steering system structure, the most used topologies of electric power steering and the advantages of using brushless DC motors for electric power steering assistance. An electric power steering architecture is proposed. The method of design the brushless DC motor for this electric power steering is presented. Design of the brushless DC motor was based on the analysis of the requirements of the EPS systems, analysis of the control methods, modelling and simulation in MATLAB/SIMULINK. Simulation for six various conditions are presented and analysed for optimal sizing of the electric motor. An experimental model of the designed motor has been manufactured for validation.

Keywords: Simulation analysis, Brushless motor, Electric Power Steering, Permanent magnets, Optimal Design, Control methods

Received: *14 April 2020*

To cite this article:
CIOBOATĂ D., NEACȘU M.G., STANCIU D., MATEI S.Șt., NEACȘU I., "Modelling and Simulation of a Brushless DC Motor for Electric Power Steering Assistance", in Electrotehnica, Electronica, Automatica (EEA), 2020, vol. 68, no. 3, pp. 22-31, ISSN 1582-5175. https://doi.org/10.46904/eea.20.68.3.1108003

1. Introduction

In recent years, brushless DC motors (BLDCs) have started to be used frequently in many applications in automotive industry, such as electric vehicles drive systems, electric power steering, air conditioner, engine cooling, etc.

Joanne Goh's analyses on the evolution of the market share for different electric motors used in the automotive industry, for the 2016–2021 time frame, highlight that the growth rate of BLDCs sales is higher than that of DC brushed motors and stepper motors [1], [13].

The global brushless DC motor market size is expected to reach over $ 15.000 million in 2021, from about $ 12,000 million in 2016.

The steering system is one of the most important and complex system installed on a vehicle. Steering system provides the directional change in the movement of an automobile. This system converts the rotation of the steering wheel into angular movement of the front wheels to control the direction of the vehicle motion.

In recent developments, in automotive industry, the trend is that electrical power steering (EPS) replaces the hydraulic power steering (HPS). EPS offers several advantages over conventional HPS, such as improved fuel economy (because the electric motor is driven only when the steering wheel is turned), elimination of hydraulic fluid and eliminates many components such as the pump, hoses, fluid, drive belt and pulley. For this reason, electric steering systems tend to be smaller and lighter than hydraulic systems [2], [3].

One of the main parts of the EPS is the electric motor, typically a BLDC motor, which replace the hydraulic actuation mechanism to develop the required steering torque.

Many research and technical papers on the EPS system and BLDC motors have been published, relating to basic principle and control algorithms and strategies, method for operating the brushless electric motors, permanent magnets, inverters for actuating brushless motors, BLDC rotor position control method [2]-[6]. Various EPS systems were modelled and analysed. Most articles refer to column type EPS [7]-[9], [23]-[25].

However, the topic is still of interest, in order to improve and optimize the BLDC motors and EPS systems performances.

Current research areas are:

- improvement of manufacturing materials and technologies;
- power electronic drivers;
- feedback sensors;